**Rare Metal Materials and Engineering**
Volume 54, Issue 5, May 2025
Available online at www.rmme.ac.cn

Science Press

**Cite this article as**: Wang Fanghui, Li Hushan, Zhang Hao, et al. Effect of Current Density and Strain Rate on Deformation Resistance During Electrically-Assisted Compression of $AlCr_{1.3}TiNi_2$ Eutectic High-Entropy Alloys[J]. Rare Metal Materials and Engineering, 2025, 54(05): 1121-1126. DOI: https://doi.org/10.12442/j.issn.1002-185X.20240561.

LETTER

# Effect of Current Density and Strain Rate on Deformation Resistance During Electrically-Assisted Compression of $AlCr_{1.3}TiNi_2$ Eutectic High-Entropy Alloys

**Wang Fanghui[1,2,3], Li Hushan[1,2,3], Zhang Hao[1,3], Ding Ziheng[1,2,3], Bao Jianxing[4], Ding Chaogang[1,2,3], Shan Debin[1,2,3], Guo Bin[1,2,3], Xu Jie[1,2,3]**

*[1] Key Laboratory of Micro-systems and Micro-structures Manufacturing, Ministry of Education, Harbin Institute of Technology, Harbin 150001, China; [2] National Key Laboratory for Precision Hot Processing of Metals, Harbin Institute of Technology, Harbin 150001, China; [3] School of Materials Science and Engineering, Harbin Institute of Technology, Harbin 150001, China; [4] Xi'an Rare Metal Materials Institute Co., Ltd, Xi'an 710016, China*

**Abstract:** The effect of deformation resistance of $AlCr_{1.3}TiNi_2$ eutectic high-entropy alloys under various current densities and strain rates was investigated during electrically-assisted compression. Results show that at current density of 60 A/mm$^2$ and strain rate of 0.1 s$^{-1}$, the ultimate tensile stress shows a significant decrease from approximately 3000 MPa to 1900 MPa with reduction ratio of about 36.7%. However, as current density increases, elongation decreases due to intermediate temperature embrittlement. This is because the current induces Joule effect, which then leads to stress concentration and more defect formation. Moreover, the flow stress is decreased with the increase in strain rate at constant current density.

**Key words:** eutectic high-entropy alloy; electrically-assisted compression; deformation resistance; flow stress

## 1 Introduction

High-entropy alloys (HEAs) have garnered significant attention in recent years due to their exceptional mechanical properties, which make them suitable for a wide range of advanced applications[1–5]. Among various developed HEAs, eutectic HEAs (EHEAs) are particularly notable. These alloys, which feature a unique combination of both soft and hard phases, stand out because of their eutectic microstructures[6–8]. This specific microstructural configuration allows EHEAs to exhibit remarkable mechanical properties, including excellent tensile strength at room temperature, which can be attributed to their distinctive diphase lamellar microstructure[6]. Despite these advantages, the high production cost of cobalt-containing EHEAs poses a significant barrier to their widespread use in practical engineering applications. EHEAs without cobalt (Co-free EHEAs), on the other hand, are more cost-effective alternatives, thereby attracting much attention for practical applications where budget constraints are a concern[9]. In light of limited budget, Wang et al[10] developed a new Co-free $AlCr_{1.3}TiNi_2$ EHEA, aiming to provide a lightweight cost-efficient alternative with excellent mechanical performance. The $AlCr_{1.3}TiNi_2$ EHEA demonstrates superior hardness and high specific yield strength at a wide temperature range from ambient temperature to high temperature, compared with many other EHEAs. Although the ultra-high strength of these alloys offers certain advantages, it also leads to high deformation resistance, resulting in more challenges for the deformation process and thereby raising the susceptibility to rupture during mechanical processing or

Received date: August 29, 2024
Foundation item: National Natural Science Foundation of China (52305349); Heilongjiang Touyan Team (HITTY-20190036); Heilongjiang Provincial Natural Science Foundation of China (LH2023E033); CGN-HIT Advanced Nuclear and New Energy Research Institute (CGN-HIT202305); Natural Science Basic Research Program of Shaanxi Province (2023-JC-QN-0518)
Corresponding author: Ding Chaogang, Ph. D., Assistant Researcher, School of Materials Science and Engineering, Harbin Institute of Technology, Harbin 150001, P. R. China, E-mail: dingcg@hit.edu.cn

application.

Fortunately, electrically-assisted deformation (EAD) presents a promising approach to mitigate those effects to a certain extent. By applying an electric current during the deformation process, EAD effectively reduces flow stress, thereby enhancing the formability and reducing the possibility of rupture[11–14]. The particular effectiveness of this technique is due to the Joule effect. Currently, EAD has been widely used, particularly in the fields of roll forming[12], micro-forming[15], micro-embossing[16], and blanking[17]. By EAD technique, Bao et al[15] obtained titanium alloy micro-gear with excellent performance and smooth surface.

Wang et al[18] demonstrated that the Joule effect is the predominant factor influencing stress reduction during EAD, contributing up to 90% of the observed reduction. This finding underscores the importance of the thermal effects induced by electric currents in the alteration of mechanical properties of HEAs. Yang et al[19] reported a substantial decrease in the ultimate tensile stress (UTS) of $Al_{0.6}CoCrFeNiMn$ HEA, which was decreased from approximately 900 MPa to 400 MPa when the current density was 60 A/mm$^2$. This notable decrease in UTS highlights the effectiveness of EAD in enhancing the ductility of HEAs by reducing the strength and thereby facilitating deformation process. Furthermore, Wang et al[20] observed that localized Joule heat led to an increase in the temperature of $CoCrFeNiW_{0.5}$ HEA during electrically-assisted compression (EAC), resulting in a significant reduction (50%) in yield strength (YS), which promotes deformation under compression. This phenomenon is highly beneficial for applications requiring extensive shaping or forming of these alloys. In addition to YS reduction, the Joule effect caused by electric current also plays a crucial role in reducing stress concentration within the materials. This reduction in stress concentrations is essential, as it minimizes the formation of cracks and other defects that may compromise the alloy integrity during mechanical processing[19–20].

Extensive research has consistently demonstrated the effectiveness of electric current in reducing deformation resistance during the deformation process of various HEAs. It has been proven that this approach is particularly effective to overcome the inherent challenges associated with the high strength and deformation resistance of these advanced materials. However, despite the potential benefits of EAD, the specific case of $AlCr_{1.3}TiNi_2$ EHEA presents unique challenges. The high strength and significant deformation resistance make it particularly difficult to deform, and rare research was conducted on the application of EAD to this specific material. In response to this gap in the research field, EAC experiments were conducted on $AlCr_{1.3}TiNi_2$ EHEA to investigate its deformation resistance under various current densities and strain rates. The primary objective of these experiments was to explore the potential of flow stress reduction through the application of electrical current during the deformation process. The analysis of the mechanical properties of $AlCr_{1.3}TiNi_2$ EHEA during EAC process revealed a significant reduction in peak stresses, indicating a decrease in deformation resistance as the electric current was applied.

However, this study also found that although the application of electric current was effective in reducing peak stresses, excessively high current densities led to intermediate temperature embrittlement due to the Joule effect. This unintended consequence resulted in a reduction in ductility, which thereby restricted the extent of safe deformation without the fracture risk. The intermediate temperature embrittlement, caused by localized heating from the electric current, highlights the need for careful optimization of current density during EAC to balance the benefits of stress reduction against the potential for embrittlement and reduced ductility. This research investigated the effect of deformation resistance of $AlCr_{1.3}TiNi_2$ EHEA under different conditions during electrically-assisted compression.

## 2 Experiment

An ingot (5 kg) of $AlCr_{1.3}TiNi_2$ EHEA was prepared by high-purity raw metals (purity more than 99.99%) via electromagnetic levitation melting in an argon atmosphere. To ensure better compositional homogeneity, the ingot was remelted 5 times. Afterwards, the ingot was furnace-cooled to about 150 °C and then air-cooled.

The phase structure was analyzed by X-ray diffraction (XRD) with Cu Kα radiation at 45 kV. Microstructural characterization was conducted using scanning electron microscope (SEM, Quanta 200FEG, USA), and chemical element distribution was further examined via energy dispersive spectroscope (EDS). EAC experiments were conducted on the specimens with 2.5 mm in diameter and 3.75 mm in height, using a universal testing machine (Instron 5530, USA, 50 kN) with current supplied by a pulsed power supply (MicroStar CRS-LFP12-500, Dynatronix Inc). The maximum output current and maximum output power were 500 A and 10 kW, respectively. The positive and negative poles of power supply were connected to the upper die and the lower die, respectively, and the bakelite plates were used to insulate the electricity. Fig. 1 shows the schematic diagram of EAC equipment. Additionally, an infrared thermography camera (FLIR T660, USA) was employed to capture images to illustrate temperature field variation. Prior to testing, the

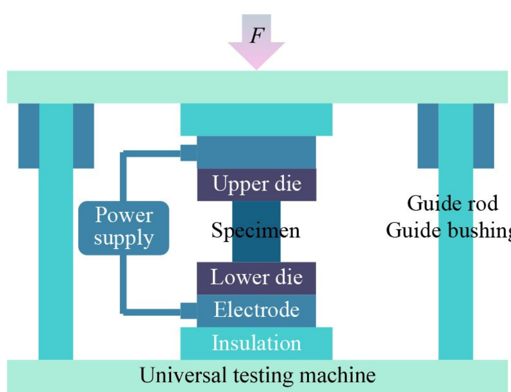


Fig.1 Schematic diagram of EAC platform

surface was sprayed with black heat resistant paint to obtain uniform emissivity.

## 3 Results and Discussion

The phase identification of the $AlCr_{1.3}TiNi_2$ EHEA was analyzed by XRD, as shown in Fig.2. It can be observed that the diffraction peaks correspond to both $L2_1$ phase and body-centered cubic (bcc) phase. This observation is consistent with the results in Ref. [10], confirming the presence of these phases in $AlCr_{1.3}TiNi_2$ EHEA.

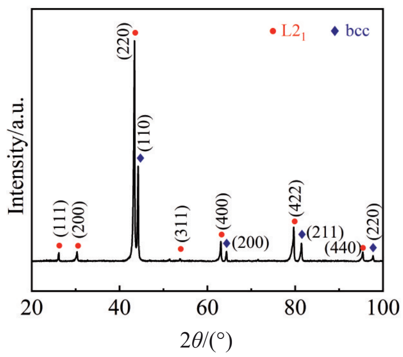


Fig.2 XRD pattern of as-cast $AlCr_{1.3}TiNi_2$ EHEA

According to Fig. 2, low-angle diffraction peaks can be observed at $2\theta$=26° and 30°, which are identified as the characteristic peaks of $L2_1$ phase. Specifically, these peaks at $2\theta$=26° and 30° correspond to the (111) and (200) crystallographic planes of $L2_1$ phase, respectively. The strongest diffraction peak associated with the $L2_1$ phase can be detected at approximately $2\theta$=44°, which corresponds to the (220) plane, indicating a high degree of crystallinity and the presence of $L2_1$ phase within the alloy.

Adjacent to this strongest peak of $L2_1$ phase, another prominent peak can be observed, corresponding to the (110) plane of bcc phase. The proximity and intensity of these peaks suggest a closely related structural arrangement between the $L2_1$ and bcc phases in the alloy. The presence of both $L2_1$ and bcc phases contributes to the unique mechanical properties of the $AlCr_{1.3}TiNi_2$ EHEA, acting as a crucial role to determine the strength, ductility, and overall performance of alloys.

Fig. 3 illustrates the microstructure of $AlCr_{1.3}TiNi_2$ EHEA. As shown in Fig.3a–3d, the $AlCr_{1.3}TiNi_2$ EHEA predominantly exhibits a homogeneous ultrafine laminar structure, which is characterized by alternating layers of different phases at nanoscale. This feature provides the material with unique mechanical properties, such as high strength and high tough-

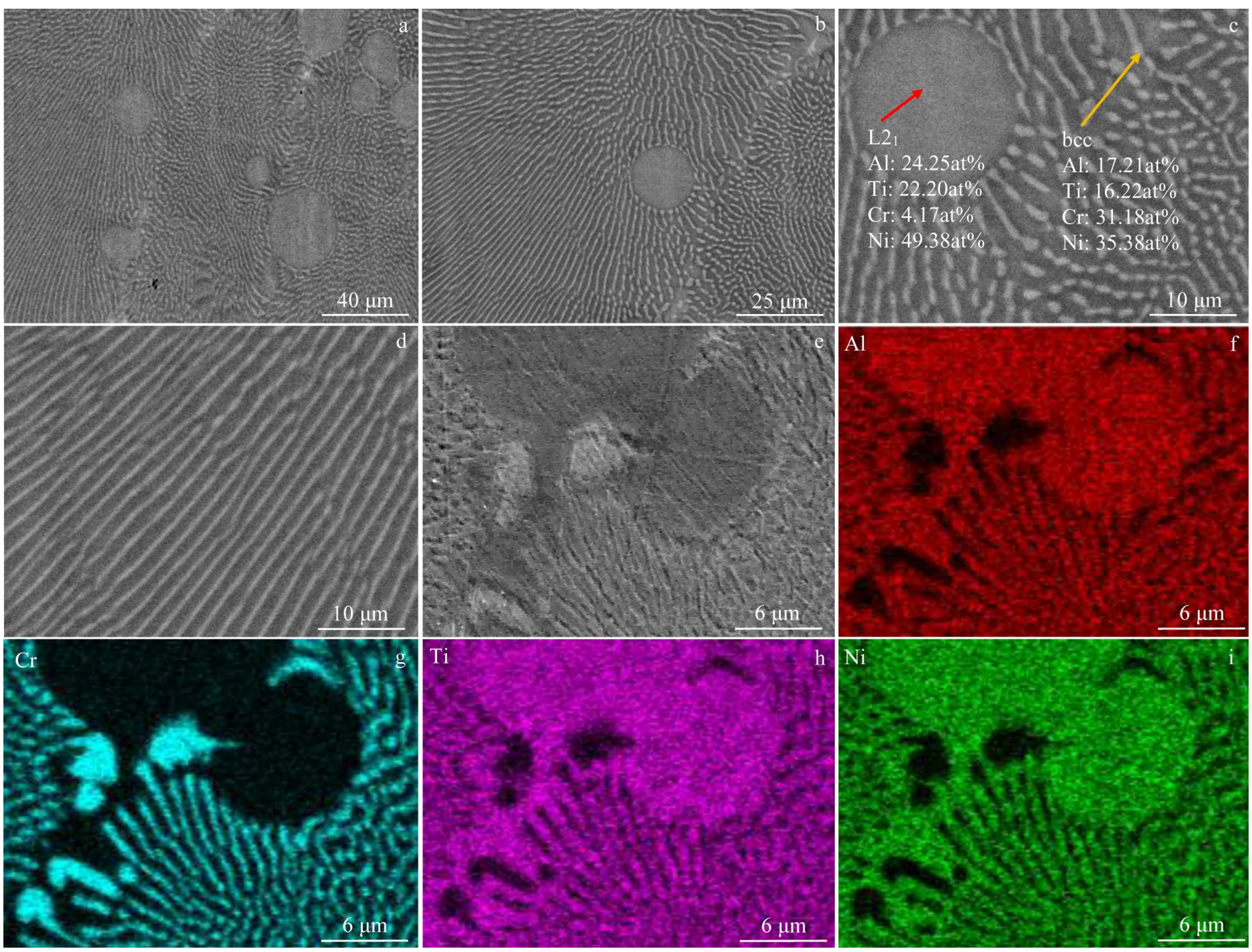


Fig.3 SEM images of $AlCr_{1.3}TiNi_2$ EHEA (a–d); SEM image (e) and corresponding EDS element mappings (f–i) of $AlCr_{1.3}TiNi_2$ EHEA

ness. This observation aligns well with the results in Ref.[10]: ultrafine lamellar structure can be observed in the alloy.

Furthermore, the element distributions within the alloy are depicted in Fig.3f–3i. Spatial distribution of key elements can be found, and element segregation occurs. Notably, sub-circular regions can be observed, which are indicative of the areas where certain elements are segregated or concentrated, leading to localized composition variations. The chemical composition of these regions is presented in Fig. 3c, further elaborating on the specific elements present in different areas of the microstructure.

Consistent with the findings in Ref. [10], this analysis also reveals that the lamellar microstructure and the surrounding matrix are enriched with different elements depending on the phase. Specifically, the regions corresponding to bcc phase are enriched with Cr, whereas the lamellae associated with the $L2_1$ phase are enriched with Al, Ti, and Ni. This element partitioning can also be confirmed through SEM-EDS analysis, which corroborates the distribution patterns. The distinct segregation of elements within these phases contributes to the unique mechanical properties of the alloy by influencing the strength, hardness, and overall stability of the material.

The temperature field variations of $AlCr_{1.3}TiNi_2$ EHEA during EAC are illustrated in Fig.4. The temperature variation can be categorized into four stages: (I) initial temperature distribution, (II) establishment of initial steady-state temperature, (III) onset of crack initiation, and (IV) progression of crack extension.

With the application of electric current, the temperature of the specimen rapidly increases from ambient temperature, leading to stage I—the temperature variation process. This initial rise in temperature is primarily due to Joule heating, which occurs as the electric current passes through the conductive material. After a short period, a dynamic thermal equilibrium is achieved, representing the stage II. At this point, the rate of heat generated by Joule heating is balanced against the rate of heat loss through thermal radiation and conduction, bringing the specimen temperature to a steady state. As the process continues, the stage III is characterized

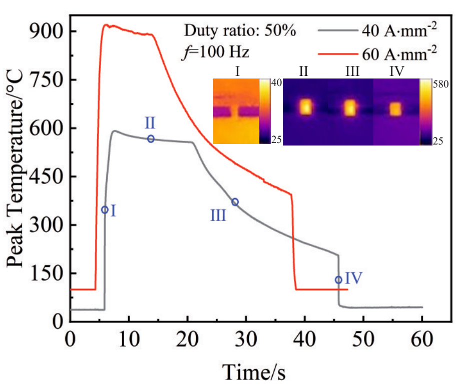


Fig.4 Variations of temperature field with time and current density during EAC

by a gradual increase in temperature. This increase persists until the onset of crack initiation, which is evidenced by a noticeable change in the cross-sectional area of the specimen, indicating localized weakening and stress concentration. At this stage, the material begins to exhibit the signs of structural failure due to the continuous rise in temperature and the associated reduction in material strength. Eventually, the temperature reaches its peak just before the occurrence of fracture (the stage IV). During this stage, cracks begin to propagate and extend, and the structural integrity of the material is severely damaged, leading to a rapid decrease in temperature. This drop is attributed to the reduced energy dissipation through heating as the material starts to break apart and loses continuity.

To provide a clearer representation of the temperature field variations, Fig. 4 also shows the temperature changes at a constant strain rate of 0.01 $s^{-1}$ under different current densities (40 and 60 $A/mm^2$). The results indicate that with the increase in the current density, the peak temperature also increases. Specifically, under EAC conditions, peak temperatures of approximately 580 and 900 °C can be reached when the current densities are set as 40 and 60 $A/mm^2$, respectively. This finding suggests that higher current densities lead to greater Joule heating, which significantly raises the peak temperatures. The correlation between current density and peak temperature is critical to understand the thermal and mechanical responses of the alloy during deformation process, which also highlights the need for careful control of current density to avoid excessive heating and potential material failure.

The compression behavior of the material was investigated under different current densities (40 and 60 $A/mm^2$) and strain rates ($10^{-1}$ and $10^{-2}$ $s^{-1}$). The engineering stress-engineering strain curves are depicted in Fig. 5a. In comparison to static compression tests conducted without applying any electrical current, EAC process exhibits a progressive reduction in flow stress. Specifically, the peak stress experiences a noticeable decrease as the current density increases. For instance, UTS drops from approximately 3000 MPa to 1900 MPa, reflecting a significant reduction of about 36.7%. This reduction in stress is primarily attributed to stress softening, which is a phenomenon induced by Joule heating effects resulting from the electric current. This finding is in alignment with the results in Ref.[18–19].

Interestingly, the elongation decreases with the increase in current density during EAC, which is different from the conventional electroplasticity effect where the enhancement in ductility typically occurs. Previous reports have attributed this unexpected behavior to intermediate temperature embrittlement[20–21]. As current density rises, localized Joule heating intensifies at the interfaces within the material. In the case of the $AlCr_{1.3}TiNi_2$ EHEA, the small-scale internal lamellar microstructure results in a higher density of interfaces. This heightened interface density exacerbates localized Joule heating, amplifying stress concentrations at defects. Consequently, this phenomenon promotes the

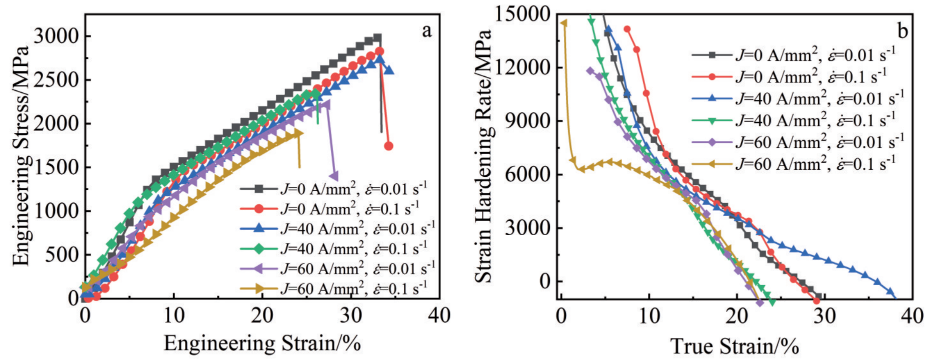


Fig.5 Engineering stress-engineering strain curves (a); strain hardening rate curves with true strain (b)

initiation and expansion of micropores, which in turn leads to a reduction in elongation[20].

Additionally, the influence of varying strain rates on compression behavior is also examined. It can be observed that higher strain rates lead to a decrease in peak stress. This is because during EAC at a constant current, the cross-sectional area of the specimen increases as strain progresses. Consequently, the effective current density through the specimen diminishes. Moreover, increasing the strain rate shortens the duration of heat transfer, resulting in less heat loss to surrounding materials. As a result, the temperature within the specimen rises more significantly at high strain rates, which is a key factor contributing to the observed peak stress reduction and associated strain rate softening phenomenon of the material[20,22].

Further analysis results of the strain hardening rate as a function of true strain under various current densities and strain rates are presented in Fig. 5b. It can be seen that the work hardening rate decreases rapidly with the increase in true strain. However, at current density of 60 A/mm$^2$ and strain rate of 0.1 s$^{-1}$, the work hardening rate exhibits a complex behavior. Initially, there is a sharp decline at low true strain, followed by a notable increase up to a certain strain degree. Afterwards, it decreases sharply again. This fluctuation in the work hardening rate is attributed to the extensive deformation behavior occurring during EAC at high strain rates, which can significantly affect the work hardening characteristics of materials[23].

## 4 Conclusions

1) Due to the Joule effect produced by the current, stress softening occurs and thus UTS decreases by about 36.7%.

2) The size of the internal lamellar microstructure is too small, leading to excessive density of internal interfaces. This phenomenon produces intermediate temperature embrittlement, leading to a ductility reduction during EAC.

## References

1 Li Jianbo, Wan Gang, Wu Bo *et al. Rare Metal Materials and Engineering*[J], 2023, 52(4): 1184

2 Liu D, Jin X, Guo N *et al. Materials Science and Engineering A*[J], 2021, 818: 141386

3 Qi Yuming, Xu Heming, He Tengwu *et al. Materials Science and Engineering A*[J], 2021, 814: 141196

4 Chen Qiushi, Dong Yong, Zhang Junjia *et al. Rare Metal Materials and Engineering*[J], 2017, 46(3): 651

5 Jiang Wentao, Wang Ye, Jiang Bo *et al. Rare Metal Materials and Engineering*[J], 2023, 52(3): 846

6 Huang Liufei, Sun Yaoning, Chen Na *et al. Materials Science and Engineering A*[J], 2022, 830: 142327

7 Huang Yifei, Chen Xizhang, Ma Shengguo *et al. Materials Letters*[J], 2024, 363: 136312

8 Lu Yiping, Dong Yong, Guo Sheng *et al. Scientific Reports*[J], 2014, 4(1): 6200

9 Jin Xi, Bi Juan, Zhang Lu *et al. Journal of Alloys and Compounds*[J], 2019, 770: 655

10 Wang Mingliang, Lu Yiping, Wang Tongmin *et al. Scripta Materialia*[J], 2021, 204: 114132

11 Zhang Xiaoli, Yan Siliang, Meng Miao *et al. Materials Science and Engineering A*[J], 2023, 864: 144573

12 Shan D, Li H, Chen Y *et al. Journal of Netshape Forming Engineering*[J], 2024, 16(7): 23

13 Li Hushan, Ding Chaogang, Ding Ziheng *et al. Rare Metal Materials and Engineering*[J], 2024, 53(10): 2713

14 Li H, Cao Y, Zhu X *et al. Journal of Netshape Forming Engineering*[J], 2024, 15(7): 1

15 Bao Jianxing, Xu Jie, Qu Jiazheng *et al. Journal of Mechanical Engineering*[J], 2021, 57(1): 210

16 Wang Xinwei, Xu Jie, Wang Chunju *et al. Materials*[J], 2020, 13(2): 412

17 Tang Zejun, Du Hao, Lang Lihui *et al. Journal of Materials Processing Technology*[J], 2018, 253: 86

18 Wang Xinwei, Xu Jie, Shan Debin *et al. International Journal of Plasticity*[J], 2016, 85: 230

19 Yang Zhiqin, Bao Jianxing, Ding Chaogang *et al. Journal of Materials Science & Technology*[J], 2023, 148: 209

20 Wang Pei, Wu Weichao, Cui Fei *et al. Materials Characterization*[J], 2023, 202: 112981

21 Jiang Z L, Zeng Q, Anderoglu O *et al. Materials Science and Engineering A*[J], 2019, 745: 484

22 Bao Jianxing, Chen Wanji, Bai Jianan *et al*. *Materials Science and Engineering A*[J], 2022, 831: 142262

23 Zhang Zhen, Xie Yuehuang, Liang Jiamiao *et al*. *Intermetallics*[J], 2024, 167: 108238

# 电流密度和应变速率对$AlCr_{1.3}TiNi_2$共晶高熵合金电压缩抗变形性能的影响

王方辉[1,2,3]，李虎山[1,2,3]，张　浩[1,3]，丁子恒[1,2,3]，包建兴[4]，丁朝刚[1,2,3]，
单德彬[1,2,3]，郭　斌[1,2,3]，徐　杰[1,2,3]

(1. 哈尔滨工业大学 微系统与微结构制造教育部重点实验室，黑龙江 哈尔滨 150001)
(2. 哈尔滨工业大学 金属精密热加工国家级重点实验室，黑龙江 哈尔滨 150001)
(3. 哈尔滨工业大学 材料科学与工程学院，黑龙江 哈尔滨 150001)
(4. 西安稀有金属材料研究院有限公司，陕西 西安 710016)

**摘　要**：研究了不同电流密度和应变速率下$AlCr_{1.3}TiNi_2$共晶高熵合金在电辅助压缩过程中抗变形性能的影响。结果表明：当电流密度为60 A/mm$^2$，应变速率为0.1 s$^{-1}$时，抗拉伸强度显著降低，从约3000 MPa降至1900 MPa，降幅约36.7%。然而，随着电流密度的增加，由于中温脆性延伸率下降，这是由于电流引起的焦耳效应导致应力集中，缺陷形成增加。在恒定电流密度下，流变应力随应变速率的增大而减小。

**关键词**：共晶高熵合金；电辅助压缩；抗变形性能；流动应力

作者简介：王方辉，男，2000年生，硕士生，哈尔滨工业大学材料科学与工程学院，黑龙江 哈尔滨 150001，E-mail：wangfanghui1014@163.com